



## Petrographic and geochemical features of Gimo marble, Gole area, Kurdistan Region, Iraq: constraints on its protolith's origin and depositional environment

Tola Ahmed Mirza<sup>1</sup>, Stavros P. Kalaitzidis<sup>2</sup>, Sardar S. Fatah<sup>1</sup>, Sophia Tsiotou<sup>2</sup>

<sup>1</sup>University of Sulaimani, Iraq.

<sup>2</sup>Department of Geology, University of Patras, GR-26504, Rio-Patras, Greece

Corresponding author: tola.merza@univsul.edu.iq

### ABSTRACT

It is essential to identify marbles' petrographic and geochemical characteristics to determine the palaeo-environmental settings where their carbonate protoliths formed. The petrogenesis of massive Gimo marbles in the Gole area, Kurdistan Region of northeast Iraq, was investigated in this study through a combination of field mapping, petrographic, and geochemical techniques. Petrographic examination of these marbles reveals that mineral compositions are similar in all samples, with both homeoblastic and mosaic textures occurring, in addition to opaque grains that provide evidence of mineralization. Geochemical analyses show that the average calcium carbonate content of the marble is 94.96%; hence, the marble is lithologically characterized as a pure calcite marble. In most samples, the silica content was below 2 wt.%, with high values related to quartz veinlets. A range of geochemical indices and Post-Archean Australian Shale (PAAS-normalized rare earth element (REE) patterns) suggest that the limestone protolith was deposited in a shallow, near-shore marine environment on a continental margin, with very low input of detrital material. The negative Ce anomalies indicate that the protoliths of the Gimo marbles were carbonate rocks of a sedimentary origin.

*Keywords: Gimo marble; Kurdistan Region; homeoblastic; mosaic texture;*

## Características petrográficas y geoquímicas de los mármoles de Gimo, en el Kurdistan iraquí: limitaciones en el origen y ambiente deposicional de sus protolitos

### RESUMEN

Este artículo parte de la importancia de identificar las características geoquímicas y petrográficas de los mármoles para determinar la configuración paleoambiental donde se formaron sus protolitos carbonatados. En este estudio se investigó la petrogenesis de los mármoles masivos de Gimo, en el área de Gole, región del Kurdistan en el noreste iraquí, a través de la combinación de mapeo de campo, con técnicas petrográficas y geoquímicas. El examen petrográfico de estos mármoles revela que las composiciones minerales son similares en todos los ejemplos, tanto con texturas homeoblásticas como mosaicas y con adición de granos opacos que ofrecen evidencias de la mineralización. Los análisis geoquímicos muestran que el contenido promedio de calcio carbonatado del mármol es de 94.96 %, lo que significa que estas muestras se caracterizan litológicamente como mármoles de calcita pura. En muchos de los ejemplos, el contenido de sílice fue inferior a 2 wt%, con altos valores relacionados a vetillas de cuarzo. Una gama de índices geoquímicos y Esquistos Australianos Posarcaicos (PAAS, en inglés; patrones de elementos tierras raras normalizados) sugieren que los protolitos de caliza se alojaron en un ambiente somero en el margen continental cercano a la línea costera, con un ingreso de contenido de detritos muy bajo. Las anomalías negativas de cerio indican que los protolitos de los mármoles de Gimo fueron rocas carbonatadas de origen sedimentario.

*Palabras clave: mármoles de Gimo; región del Kurdistan; textura homeoblástica; textura mosaica.*

### Record

Manuscript received: 29/06/2020

Accepted for publication: 05/02/2021

### How to cite item

Mirza, T. A., Kalaitzidis S. P., Fatah S. S., Tsiotou S. (2021). Petrographic and geochemical features of Gimo marble, Gole area, Kurdistan Region, Iraq: constraints on its protolith's origin and depositional environment. *Earth Sciences Research Journal*, 25(3), 275-285. DOI: <https://doi.org/10.15446/esrj.v25n3.88686>

## 1. Introduction

The Iraqi marbles of Mawat and Penjween (Gimo group) are located in the extreme northeast of Iraq, near the border with Iran (Figs. 1 and 2). According to the tectonic classification of Buday and Jassim (1987), these Marbles are located in the Suture Zone of the Penjween Walsh Subzone of Central Zone of the Euogeosyncline.

The Gimo group comprises an alternation and interfingering of grey-white marble and dark grey calc-schist, with thin sheets of metabasalts in some places. This group shows a remarkable lithological resemblance to the Qandil Series from the Eocene. The Gole marble is a part of the Gimo group situated in the northeastern part of Sulaimani city at  $35^{\circ} 46' 40.68''$  N and  $45^{\circ} 49' 19.07''$  E (Figs. 1 and 2).



**Figure 1.** Satellite image of northeast Iraq showing the location of the study area near Gole village (from Google Earth).

Various studies have been carried out on the metamorphic rocks of the Penjween area, including those by Bolton (1958), Samimov and Neldov (1962), DeVilliers (1975), Jassim et al. (1982), Buday and Jassim (1987), Awadh (1991), Karim (2004), Awadh and Kettanah (2008). Most of these studies were directed towards elucidating the conditions of metamorphism. However, the metamorphic sequences in the area have not been studied in detail, and their relevance to the general geological framework remains unknown.

Jassim et al. (1982) described the metamorphic evolution of the inner zone of the Iraqi Zagros in the Bulfat, Mawat, and Penjween Massifs, suggesting that all these units were affected by the same metamorphic event, and more specifically as a result of regional metamorphism and contact metamorphism. They estimated the temperature of this contact metamorphism to be  $750^{\circ}\text{C}$  and low to medium pressure of regional metamorphism.

Karim (2004) studied the origin of the structure and textures of some Kurdistan marbles and reported plastic flow textures formed because of burial and tectonic fracturing and later filled with sparitic calcite.

Awadh and Kettanah (2008) studied the petrology and geochemistry of the Shalair Metamorphic Rock Group (SMRG) and showed that three lithological units characterize the SMRG: metapelite, metacarbonate, and meta-arenite, and that the Kater Rash Volcanic Group (KRVG) is characterized by a metaigneous series including metabasalt, metaandesite, and metarhyolitic dacite. All these rocks are regionally metamorphosed into low-grade metamorphism of the greenschist facies–chlorite zone. In addition, they suggested thermal conditions of metamorphism of about  $340\pm 20^{\circ}\text{C}$  at pressure conditions of approximately 2.5–3 Kb.

This study aims to investigate the mineralogical, geochemical characteristics of Gimo marble and determining the origin of their protolith and to provide insight into the palaeo-depositional environment of the formation and as well as provide a better understanding of the origin and geotectonic setting of this part of the Iraqi Zagros Suture Zone (IZSZ).

## 2. Geological setting

The Gole area is located approximately 20 km north of Penjween Town in the Sulaimani governorate, northeast Iraq, at  $35^{\circ} 46' 40.68''$  N and  $45^{\circ} 49'$

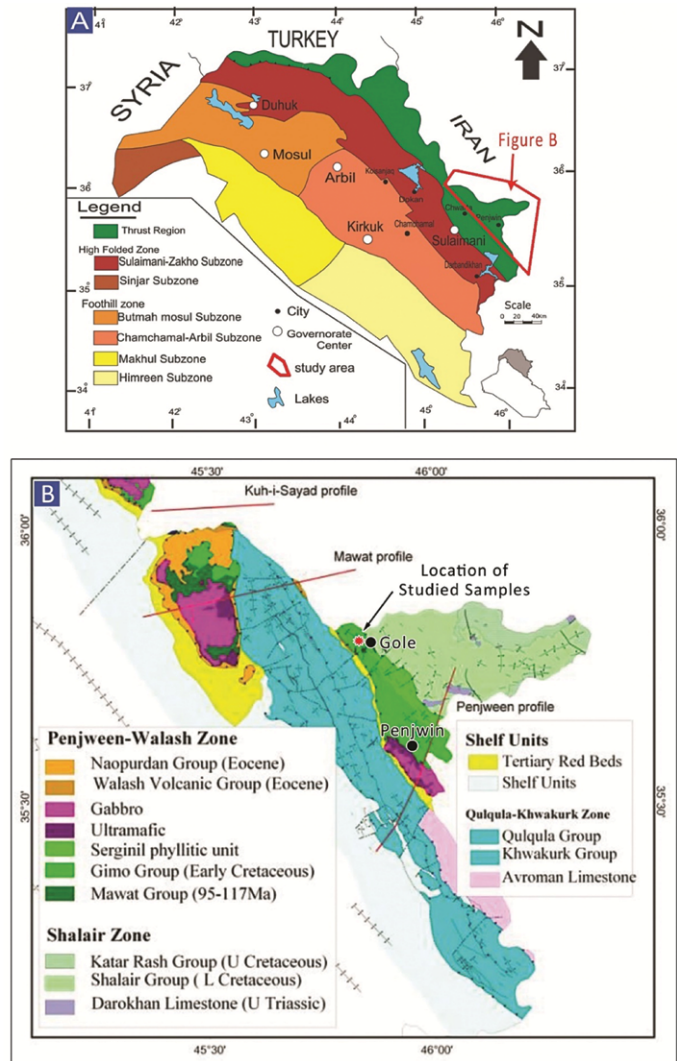


**Figure 2.** A. Geotectonic map of the Zagros Suture Zone, northeast Iraq, showing the location of the study area. B. Geological map of the Penjween area (after Jassim and Goff, 2006).

$19.07''$  E (Figs. 1 and 2). The area is geologically complex, situated within the northeastern end of the IZSZ (Fig. 2A). The Gole area belongs to IZSZ, which formed due to the collision between the Arabian passive margin and the Iranian active margin and is considered a part of the Zagros Orogenic Belt (Talbot and Alavi, 1996; Ali et al., 2016). The tectonostratigraphic units of the IZSZ preserve a complex geological record of the Arabian crust evolution during the closure of the Neo-Tethys Ocean (Jassim and Goff, 2006). The IZSZ is marked by two allochthonous thrust sheets: the upper and lower allochthonous units (Aswad, 1999; Aswad et al., 2011). The lower allochthonous unit contains volcano-sedimentary rocks of the Walsh–Naopurdan nappe, whereas the upper allochthon – or ‘ophiolite-bearing terrain’ – is represented by the Bulfat, Penjween (Gimo–Qandil Group) (Aswad, 1999; Aswad et al., 2011), and Mawat complexes of the Albian–Cenomanian (97–105 Ma) (Aswad and Elias, 1988).

The Gimo marble in the Gole area represents a part of the Qandil Metamorphic Series (QMS), which occurs in the Penjween–Walsh Sub Zone (Fig. 2B) according to the geotectonic subdivision of Iraq proposed by Buday (1980). This QMS structurally overlies the Walsh and Naopurdan Series and is composed mainly of weakly metamorphosed limestone and schist, forming the frontier range of eastern Iraq.

Buday (1980) divided the QMS into two subgroups. The lower subgroup is composed of two units: (i) the Gimo group, the lowermost unit by Buday and Blackman (1975), which includes metavolcanics interbedded with marbles, calc-schists, and phyllites; and (ii) the Sirginil group, the upper

unit, which is composed mainly of metamorphosed limestone, calc-phyllites, phyllites, and sparse conglomerates, without any volcanic admixture. The contact of the Sirginil group with the overlying sedimentary unit is erosional, whereas the contact between the Gimo and Sirginil group units is tectonic (Mirza et al., 2017; Mirza and Rashid, 2018). Based on field investigations, the exposed rocks in the study area are calcareous members of the Gimo group. This group occurs in an elongated zone, stretching from the Penjween area in the southeast to the northern parts of the Bulfat Massif (east of Qaladiza), up towards the Rawanduz river valley in the NW, and forms continuous outcrops north of the Rawanduz River. Lithologically, the Gimo

group consists of several rock units that show lateral variations; however, the main features of the group are a 600 m thick, massive, and thickly bedded layer of marble and calc-schist interbedded with basaltic lava flows (Fig. 3). The equivalent lithologies of the Gimo group in the Bulfat Massif are strongly altered by contact metamorphism, owing to intrusions of intermediate and elemental composition.

The Gimo and Sirginil sequences were hypothesized to have been formed before the Tertiary (Buday, 1980), with regional metamorphism occurring during the Late Cretaceous, causing deformation of the entire series. However, despite this tectonic disruption, the original sedimentary textures of the rocks

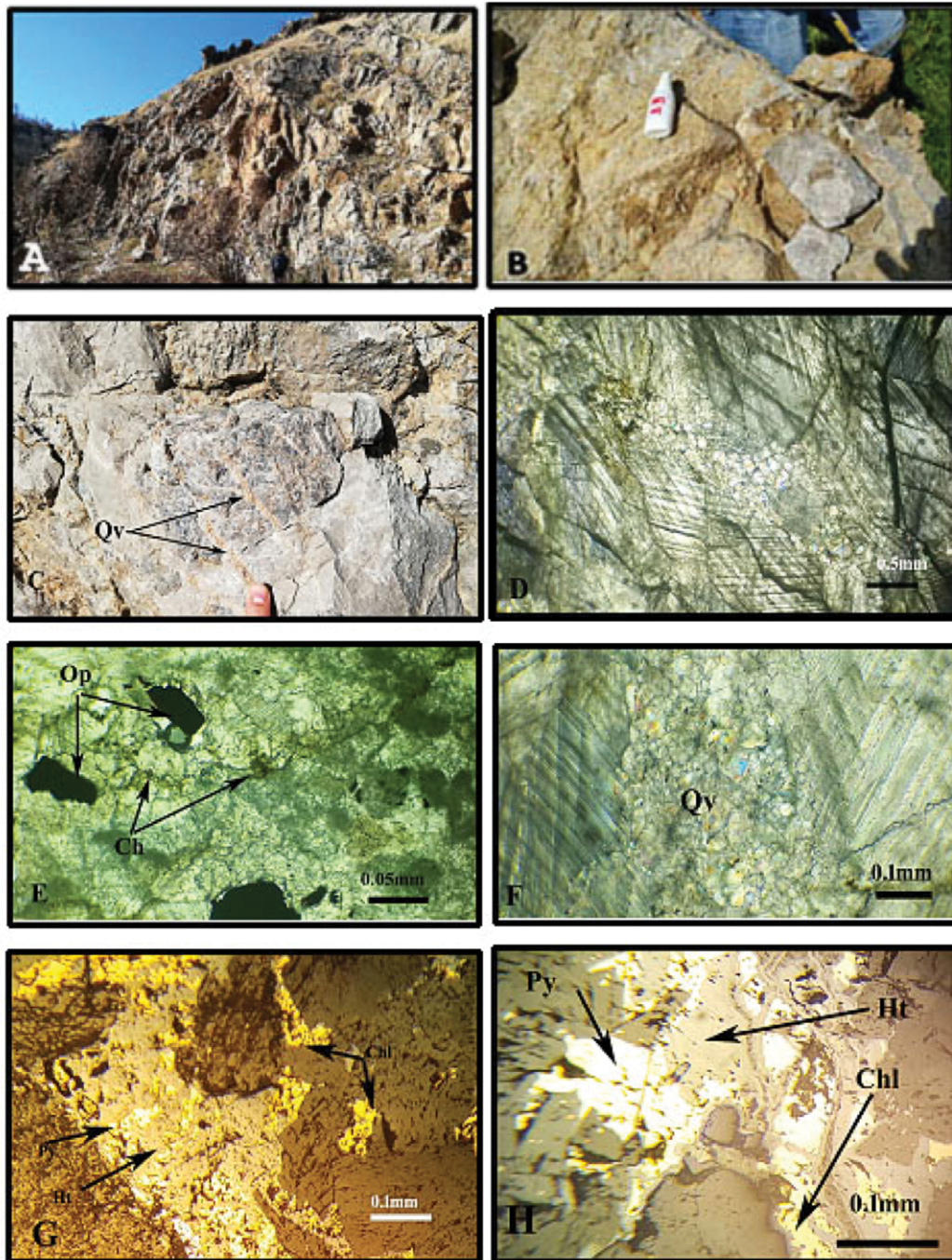


**Figure 3.** Field images and photomicrographs of Gimo marble samples. **A.** Outcrops of Gimo marble beds in the study area; **B.** field occurrence of grey-coloured calcitic marble; **C.** quartz veins that mostly show an open-space filling texture; **D.** photomicrograph of calcite grains with deformation twinning and a homeoblastic mosaic texture, shown in plane-polarised light (PPL); **E.** subhedral opaque minerals (Op); and chlorite (Ch) as accessory minerals **F.** photomicrograph of a quartz veinlet (Qv) shown in cross-polarised light (XPL); **G** and **H.** Metallic minerals associated to the Gimo marble, viewed under reflected light microscope representing hematite (Ht), Pyrite (Py) and Chalcocopyrite (Chl.)

and their primary geochemical features have mostly been preserved. The Gimo group in the Penjween area consists of massive white grey marbles, meta-tuffites, and amphibolites, which have been intruded by mafic and ultramafic rocks of the Penjween Complex. Jassim and Goff (2006) suggested that the Gimo group was deposited on seamounts in the Neo-Tethys Ocean. Thermal metamorphism around the Mawat and Penjween intrusive rocks has been described by Jassim and Al-Hassan (1977) and Buday (1980), and they have considered the metamorphism grade of the Gimo group in the Biotite zone.

### 3. Materials and methods

During fieldwork, eight 'fresh' marble samples were collected across strike within the Gimo group to investigate its petrogenesis. Six thin sections and three polished blocks were prepared at the Kurdistan Institution for Strategic Studies and Scientific Research laboratory. They were examined using a polarised-light microscope in transmitted and reflected mode to determine their

mineral contents and petrographic characteristics, respectively (i.e., mineral assemblages, associations, grain sizes, and textures).

Each fresh sample of marble was powdered through a 200 mesh in an agate mill to avoid contamination. Fused-glass discs were prepared for major element analysis by X-ray fluorescence (XRF) at the Laboratory of Electron Microscopy and Microanalysis of the Faculty of Natural Sciences, University of Patras, Greece, with a relative standard deviation percentage (RSD %) of less than 5% for all analyzed elements. Loss on ignition (LOI), which consists principally of CO<sub>2</sub> in these samples, was determined at 950 °C for 90 min.

Trace element concentrations, including rare-earth elements (REEs), were obtained at the SGS laboratory in Canada by using sodium peroxide fusion and analysis through inductively coupled plasma atomic emission spectroscopy (ICP-AES) and inductively coupled plasma mass spectrometry (ICP-MS). The detection limits for all analyzed elements in this study are presented in Tables 1, 2, and 3.

**Table 1.** Major oxide contents (wt.%) of Gimo marble samples (L.D.: Limits of Detection in %; LOI: loss on ignition, nd: not detected).

Samples	G1	G2	G3	G4	G5	G6	G7	G8	Mean	L.D %
SiO <sub>2</sub>	1.68	1.04	0.88	3.18	1.58	1.64	4.61	0.68	1.91	0.0002
Al <sub>2</sub> O <sub>3</sub>	0.06	0.11	0.05	0.03	0.17	nd	0.12	0.01	0.07	0.0002
TiO <sub>2</sub>	nd	0.01	nd	0.01	0.02	0.02	nd	nd	0.01	0.0010
CaO	53.52	54.40	54.30	51.69	53.62	52.70	51.15	54.63	53.25	0.0003
MgO	0.46	0.68	0.66	0.71	0.64	0.64	0.75	0.73	0.66	0.0010
MnO	0.03	-	-	-	-	-	-	-	-	0.0010
Fe <sub>2</sub> O <sub>3</sub>	0.22	0.14	0.12	0.12	0.13	0.14	0.30	0.12	0.16	0.0003
K <sub>2</sub> O	0.00	0.11	0.05	0.05	0.12	0.04	0.07	0.04	0.06	0.0010
Na <sub>2</sub> O	0.02	0.01	0.01	0.01	0.01	0.01	0.01	0.01	0.01	0.0010
P <sub>2</sub> O <sub>5</sub>	nd	0.07	0.04	0.07	0.06	0.03	0.04	0.11	0.05	0.0010
LOI	42.00	43.17	42.99	40.69	43.11	42.64	41.38	43.42	42.43	
Total	98.00	99.72	99.09	96.56	99.45	97.86	98.43	99.74	98.61	
CaCO <sub>3</sub> <sup>a</sup>	95.44	97.00	96.84	92.17	95.61	93.98	91.22	97.42	94.96	
MgCO <sub>3</sub> <sup>a</sup>	0.97	1.43	1.38	1.50	1.34	1.33	1.56	1.52	1.38	
SiO <sub>2</sub> /Al <sub>2</sub> O <sub>3</sub>	28.05	9.81	19.02	99.38	9.38	-	39.08	67.50	34.03	
Mg	0.28	0.41	0.40	0.43	0.38	0.38	0.45	0.44	0.40	
Ca	38.26	38.88	38.82	36.95	38.33	37.67	36.56	39.05	38.06	
Mg/Ca*100	0.73	1.06	1.02	1.16	1.00	1.02	1.23	1.12	1.04	

<sup>a</sup>: CaCO<sub>3</sub> and MgCO<sub>3</sub> values were calculated via stoichiometry

**Table 2.** Trace element contents of Gimo marble samples (ppm).

Trace elements (ppm)	G1	G2	G3	G4	G5	G6	G7	G8	Mean	D.L
Ba	8	6	5	3	4	8	7	5	5.7	2.5
Ce	6	5	10	3	6	4	8	nd	5.3	0.04
Co	4	4	4	5	3	4	5	4	4.1	0.05
Cu	27	23	4	3	18	1	5	2	10.4	0.03
Cr	4	4	3	3	3	4	3	4	3.5	0.26
Ni	18	13	15	13	15	15	19	13	15.1	0.03
Pb	1	1	1	1	1	1	1	1	1	0.09
Rb	5	4	3	3	4	4	5	3	3.9	0.12
Sr	856	258	213	245	268	288	687	246	382.6	0.04
Th	1	2	2	2	2	2	2	1	1.75	0.02
W	2	5	4	8	3	6	3	5	4.5	0.02
Y	4.5	15	14.8	15	23	21	13.2	13	14.94	1.7
Zn	17	20	9	7	18	7	10	5	11.6	0.06
Zr	6	8	9	8	9	9	21	7	9.6	0.6
Hf	3	3	3	3	3	3	3	3	3	0.02
Sr/Rb	171	65	71	82	67	72	137	82	93.375	
Sr/Ba	107	43	43	82	67	36	98	49	65.625	

**Table 3.** REE contents of Gimo marble samples (ppm).

REE (ppm)	PAAS	G1	G3	G7	Average	L.D(ppm)
La	38.00	3.10	10.30	2.90	5.43	0.1-10000
Ce	80.00	2.70	6.00	5.10	4.60	0.05-1000
Pr	8.90	0.52	2.00	0.90	1.14	0.05-1000
Nd	32.00	2.00	8.10	1.80	3.97	0.1-1000
Sm	5.60	0.40	1.60	0.38	0.79	0.1-1000
Eu	1.10	0.10	0.37	0.10	0.19	0.05-500
Gd	4.70	0.49	1.97	0.45	0.97	0.1-1000
Tb	0.77	0.07	0.28	0.05	0.13	0.05-10000
Dy	4.40	0.52	1.74	0.50	0.92	0.05-1000
Ho	1.00	0.10	0.37	0.10	0.19	0.05-500
Er	2.90	0.31	1.04	0.25	0.53	0.05-1000
Tm	0.40	0.05	0.14	0.05	0.08	0.05-500
Yb	2.80	0.20	0.90	0.18	0.43	0.1-1000
Lu	0.43	0.05	0.14	0.05	0.08	0.01-1000
∑ REE	183.00	10.61	34.95	12.81	19.46	
∑ LREE	164.50	8.72	28.00	11.08	15.93	
∑ HRRE	18.50	1.89	6.95	1.73	3.52	
∑ LRR/ ∑ HRR	8.89	4.61	4.03	6.40	5.02	
(La/Yb) <sub>N</sub>		1.14	0.84	1.19	1.06	
(La/Sm) <sub>N</sub>		1.14	0.95	1.12	1.07	
Er/Nd		0.16	0.13	0.14	0.14	
Y/ Ho		45.00	40.00	132.00	72.33	
Eu/Sm		0.25	0.23	0.26	0.25	
Sm/Yb		2.00	1.78	2.11	1.96	
(Nd/Yb) <sub>N</sub>		0.88	0.79	0.88	0.85	
(Pr/Yb) <sub>N</sub>		0.82	0.70	1.57	1.03	
Ce/Ce*		0.62	0.38	0.44	0.48	
Pr/ Pr*		1.21	1.37	1.69	1.42	
La/La*		4.87	4.84	1.20	3.64	
Gd/Gd*		1.64	1.26	5.90	2.93	
Eu/Eu*		0.52	0.48	0.56	0.52	

$Ce/Ce^* = Ce_N / (2Pr - Nd_N)$ ;  $Pr/Pr^* = Pr_N / (0.5Ce_N + 0.5Nd_N)$ ;  $La/La^* = -3La_N / (3Pr_N - 2Nd_N)$ ;  $(Eu/Eu^* = Eu_N / (Sm_N + Gd_N)0.5$ ; L.D: Limits of Detection.

## 4. Results

### 4.1. Petrographic features

Rock-forming minerals and their textures can be used to interpret the origin of metamorphic rocks as well as the settings from which those rocks were derived (Georgieva et al., 2009). Notable occurrences of marble rocks with a lensoid/massive form can be traced throughout the Gole area. The marble that outcrops in the area is inclined towards the northeast and forms medium to massive beds, which are often brecciated (Figs. 3A and B). They are also commonly traversed by quartz veins that mostly show an open-space filling texture (Fig. 3C).

The Gimo marble bodies show a clear petrographic variation, although most are massive, coarse-grained, and light grey to pale yellow or white in color (Fig 3A, and B). At the microscopic scale, they exhibit homeoblastic and

mosaic textures. The studied marble has simple mineralogy; they essentially consist of large recrystallized calcite (Fig. 3D), with secondary quartz, chlorite, and opaque minerals mostly in the form of hematite, pyrite, and chalcopyrite (Figs. 3E, F, G, and H). Optical microscopy revealed the predominance of a homeoblastic texture, with the carbonates being medium-grained (1.0–2.0 mm) or coarse-grained (>2 mm) (Fig. 3). The light grey marble at the microscopic scale is characterized by the presence of quartz veinlets (Fig. 3F).

Calcite crystals in the studied samples either show curved or straight grain boundaries, which sometimes form triple points (Fig. 3D). Deformation twin textures are also present in calcite, and comprise both crossing and lamellae twins that lie parallel to the rhomb edges (Fig. 3D). This type of twinning is common in calcite that forms in regional metamorphic environments and/or shear zones (Barker, 2014), and forms because of variable stresses and temperatures applied to the crystal after it has formed. According to Ferrill et al. (2004), the calcite twin width and its temperature of deformation are positively correlated.

## 4.2. Geochemical data

### 4.2.1. Major Oxides

The results of the geochemical analysis show the relatively high purity of the crystalline calcite (Table 1). All oxides, apart from CaO and LOI (i.e.  $SiO_2 + TiO_2 + Al_2O_3 + Fe_2O_3 + MnO + MgO + Na_2O + K_2O + P_2O_5$ ) sum to less than 6 wt.%, while CaO contents exceed 51 wt.% (Table 1). The insoluble residues, notably  $SiO_2$  (0.68–4.61 wt.%),  $Al_2O_3$  (0.00–0.17 wt.%), and  $K_2O$  (0.00–0.12 wt.%), have very low contents, and measured  $TiO_2$ , MnO, and  $Na_2O$  contents were negligible.

Bulk-rock analyses of the Gimo marble show very similar  $SiO_2$  contents of 0.68–1.68 wt.%, except for samples G4 and G7, which display higher values (3.18% and 4.61%, respectively) related to the presence of quartz veinlets (Fig. 3). The  $SiO_2/Al_2O_3$  ratio for all samples is highly variable (9.38–99.38), but is still typical of pure marble (Obasi and Ogungbuyi, 2014).

The most important major element oxides in carbonates in metamorphic terrains are CaO and MgO, which show values of 51.15–54.63 and 0.46–0.75 wt.%, respectively, in the studied samples. The major oxide contents of the Gimo marble are similar to those of calcitic-type marble and relatively pure limestone (Table 1, Fig. 4).

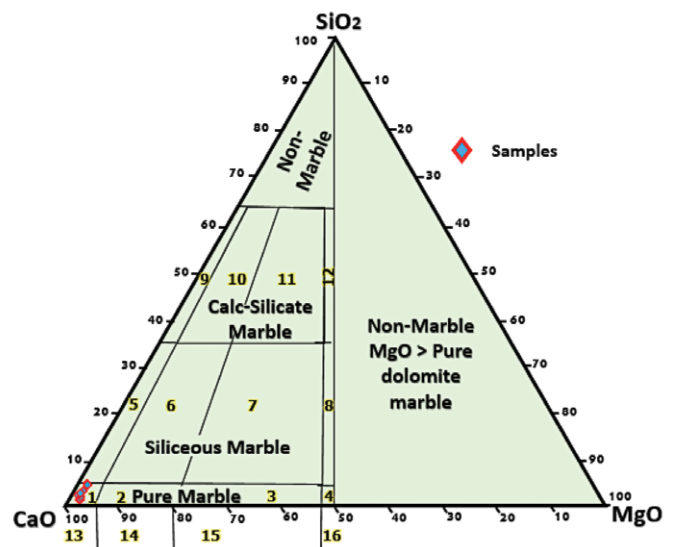


**Figure 4.** Plot of Gimo marble samples on a CaO–MgO– $SiO_2$  ternary diagram classification system (from Storey and Vos, 1981). Numbered fields are as follows: 1: pure calcite, 2: pure dolomitic calcite, 3: pure calcitic dolomite, 4: pure dolomite, 5: siliceous calcite, 6: siliceous dolomitic calcite, 7: siliceous calcitic dolomite, 8: siliceous dolomite, 9: calc-silicate calcite, 10: calc-silicate dolomitic calcite, 11: calc-silicate calcitic dolomite, 12: calc-silicate dolomite, 13: calcite marble, 14: dolomitic calcite marble, 15: calcitic dolomite marble, 16: dolomite marble, non-marble, and MgO > pure marble.

The very low MnO content in the studied samples may be attributed to the similarity in the ionic size of  $Mn^{2+}$  and  $Ca^{2+}$ , as both ions may readily substitute for each other on a crystal lattice (Ephraim, 2012). According to Goldschmidt et al. (1955), the CaO contents in calcitic marbles are usually around 50–54 wt.%, while MgO contents are <15 wt.%. The average CaO content of the Gimo marble is 53.25 wt.%, which shows that mineral phase calcite is dominant and that the protolith was a pure carbonate rock.

The LOI content varies between 40.69 and 43.42 wt.% with an average of 42.43 wt.% (Table 1), the highest values likely reflecting rocks with the lowest quartz contents. Qadhi (2008) observed that the proportion of silicate minerals, such as chlorite and quartz, in marble was negatively correlated with the LOI values of the rocks.

#### 4.2.2. Trace element

Trace element data obtained from the studied Gimo samples are summarised in Table 2, which shows that only Ba, Ce, Co, Cu, Cr, Ni, Pb, Rb, Sr, Th, W, Y, Zn, Hf, and Zr had concentrations above their detection limits. In most of these cases all measured trace elements show values mostly less than 28 ppm, apart from Sr.

In addition, the Sr, Ba, Cu, Y, and Zr contents vary significantly (Table 2), which possibly suggests a complex distribution of these elements between the samples (Georgieva et al., 2009). In the Gimo case, Sr, Ba, and Rb displayed average values of 382.6, 5.7, and 3.9 ppm, respectively, with Sr being enriched in the studied marble, as it is a typical cation that can replace Ca (Konrad and Dennis, 1995; Frimmel, 2009; Taelman et al., 2013). Shearman and Shirmohammadi (1969) considered that the Sr content of recent carbonates ranges from 30 to 200 ppm, although the average Sr concentration of the Gimo marbles (382.6 ppm) is higher than this range (Table 2). Indeed, Sr is the only trace element that showed an elevated concentration, which was particularly pronounced in samples G1 and G7 (856 and 687 ppm, respectively). Such enrichment in marble is related to  $Sr^{2+}$ , readily substituting for  $Ca^{2+}$  in limestone, with both ions having the same charge and a similar atomic radius (Konrad and Dennis, 1995). In addition, enrichment of Sr in the Gimo marbles suggests that they have not undergone significant weathering (Zhang et al., 2017).

The studied marble samples show large variations in Zr content (6–21 ppm), whereas low contents were observed for Co, Rb, Ba, Cr, Pb, Th, W, and Ni (Table 2). The post-Archean Australian Shale (PAAS; Taylor and McLennan, 1985) normalized trace element concentrations are plotted in Figure 5. The large-ion lithophile elements (LILEs) such as Rb, Ba, and Th were extremely depleted compared to PAAS. The studied samples were slightly enriched in Sr compared to PAAS. The high-field strength elements (Zr and Hf) and ferromagnesian trace elements (Co, Ni, and Cr) were depleted in all marble samples with respect to PAAS.

Rb is a large cation with a small charge that tends to be compatible with major elements, and its low ionic potential (ratio of charge to ionic radius) makes this element relatively soluble in aqueous solutions. Because of its solubility, it is quite mobile during metamorphism and weathering (Amrouni et al., 2018). According to Dypvik and Harris (2001), the enrichment of Rb in carbonate rocks is mutually associated with the presence of K-bearing minerals (clay minerals) as detrital sediment. The petrographic and geochemical observations of the Gimo marble confirm the absence of K-bearing phases as detrital sediment; hence, their impact on PAAS normalized trace element patterns (Fig. 5) can be assumed to be insignificant. Therefore, the very low Rb content in the studied samples may be related to its input during metamorphism and weathering.

Among the high field strength elements, Zr concentrations ranged from 6 to 21 ppm, with an average of 9.6 ppm, and Y concentrations range from 4.5 to 23 ppm. Average values for the transition elements with moderate to low concentrations are as follows: 15.1 ppm for Ni, 11.6 ppm for Zn, 10.4 ppm for Cu, 3.5 ppm for Cr, and 4.1 ppm for Co. In addition, Pb and Th have low average concentrations of 1 and 1.75 ppm, respectively. The presence of Th and Pb in the Gimo marble reflects their mutual association with LILEs, which are usually mobile and radioactive (Obasi and Madukwe, 2016).

The average concentrations of Cr and Ni were 3.5 and 15.1 ppm, respectively (Table 2). These values are lower than those of the PAAS, which has contents of 110 and 55 ppm, respectively (McLennan, 2001). In general,  $TiO_2$ , MnO, Cu, Pb, Zn, and Ni have an important influence on the color of

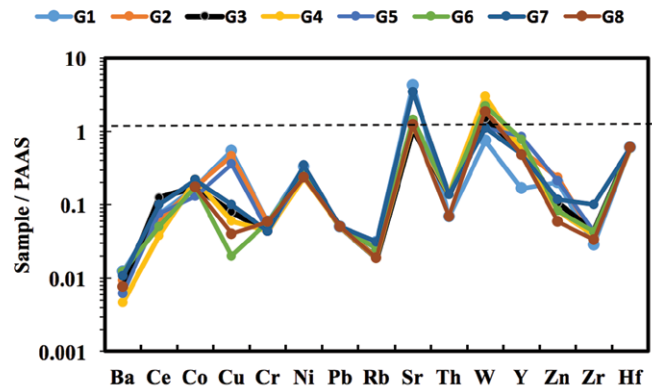


Figure 5. PAAS-normalised trace element patterns for selected Gimo marble samples using normalisation values from Taylor and McLennan (1985).

marbles; thus, their low concentrations in the studied samples explain the observed white and grey colors.

#### 4.2.3. Rare Earth Elements

The measured REE contents in the studied samples are presented in Table 3. These samples have moderate total REE ( $\Sigma$ REE) contents of 10.61–34.95 ppm, with an average of 19.34 ppm, and it is evident that light rare-earth element (LREE) components dominate over heavy rare-earth element (HREE) components, as the total concentrations of each lie within the ranges of 8.72–28.0 ppm and 1.73–6.95 ppm, respectively (Table 3).

The REE concentrations of the studied samples were normalised against PAAS (Taylor and McLennan, 1985). The normalised REE pattern diagrams are shown in Figure 6, where the following equations were used to express Eu, Pr, La, and Ce anomalies in the studied samples: (i)  $Eu/Eu^* = Eu_N / (Sm_N + Gd_N) \cdot 0.5$ , (ii)  $Pr/Pr^* = Pr_N / (0.5Ce_N + 0.5Nd_N)$ , (iii)  $La$  anomaly =  $La/La^* = La_N / (3Pr_N - 2Nd_N)$ , and (iv)  $Ce$  anomaly =  $Ce/Ce^* = 3Ce_N / (2La_N + Nd_N)$  (Bau and Dulski, 1996; Shields and Stille, 2001).

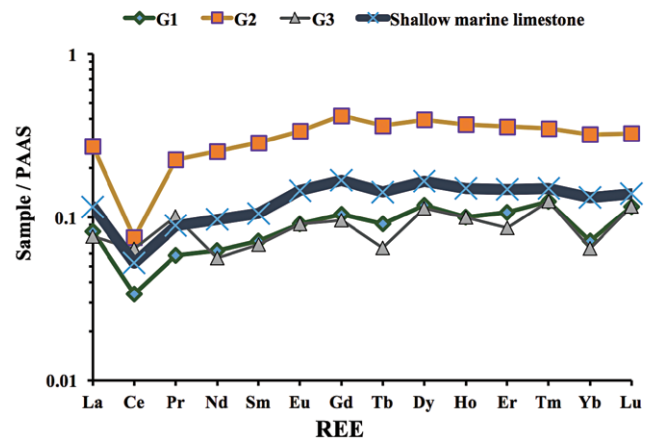


Figure 6. PAAS-normalised REE patterns for Gimo marble samples using normalisation values from Taylor and McLennan (1985).

PAAS normalized REE patterns for all samples show that HREEs are slightly enriched with  $(La/Yb)_N$  of 0.84–1.19, and  $(La/Sm)_N$  of 0.95–1.14. In all samples, the average REE content was 19.46 ppm. Ce anomalies were always negative and varied from 0.38 to 0.62.

The studied samples have variable  $\Sigma$ REEs (10.61–34.95 ppm), Y (4.5–23 ppm; ave. 14.94 ppm), and Ho (0.1 to 0.37 ppm; ave. 0.19 ppm) contents. Their Y/Ho (40.0–132.0; ave. 72.33) and Eu/Sm (0.23–0.26; ave. 0.25) ratios are similar to those of seawater, while their Sm/Yb (1.78–2.11; ave. 1.96) ratios are slightly higher than those of modern seawater (Kandemir and Yilmaz, 2009) (Table 3). Following normalisation of REEs to PAAS (Taylor and McLennan,

1985), the studied samples exhibit (i) depleted LREE relative to HREE ( $Nd/Yb)_N$  (0.79–0.88; average 0.85) and  $(Pr/Yb)_N$  (0.70–1.57; ave. 1.03), (ii) negative  $Ce/Ce^*$  (0.38–0.62; ave. 0.48), (iii) slightly positive  $Eu/Eu^*$  (0.48 – 0.56; ave. 0.52), (iv) slightly flat  $Pr/Pr^*$  (1.21–1.69; ave. 1.42) anomalies, and (v) a positive  $La/La^*$  anomaly (1.2–4.87; ave. 3.64).

## 5. Discussion

The very low MgO content of all studied samples is because of the lack of dolomite, which commonly forms owing to the replacement of Ca by Mg during metamorphism or diagenesis. This indicates that the protolith of the Gimo marble was a relatively pure limestone that was deposited in a shallow marine basin (Obasi and Ogunbunji, 2013).

Melezhik et al. (2008) suggested an Mg/Ca ratio of 0.1 as the boundary between calcite marble (CM), dolomite marble (DM), and dolomitized calcite marble (DCM). The Mg/Ca ratio of 0.5 sets a lower limit for the DM, whereas the Mg/Ca ratio of stoichiometric dolomite is 0.62. The Gole marble is characterized by variable Mg/Ca ratios ranging between 0.73 and 1.23 (Table 1, and Fig. 7A), which is greater than that of stoichiometric dolomite, therefore indicating the absence of dolomite. In addition, the plot of Ca% vs. Mg% that we used to explain the protolith of the studied samples was not affected by dolomitization. Hence, the studied samples are plotted along the limestone–dolostone mixing line (Fig. 7B) owing to very low concentrations of both Mg and  $SiO_2$  and high concentrations of Ca (Fig. 3A, and B).

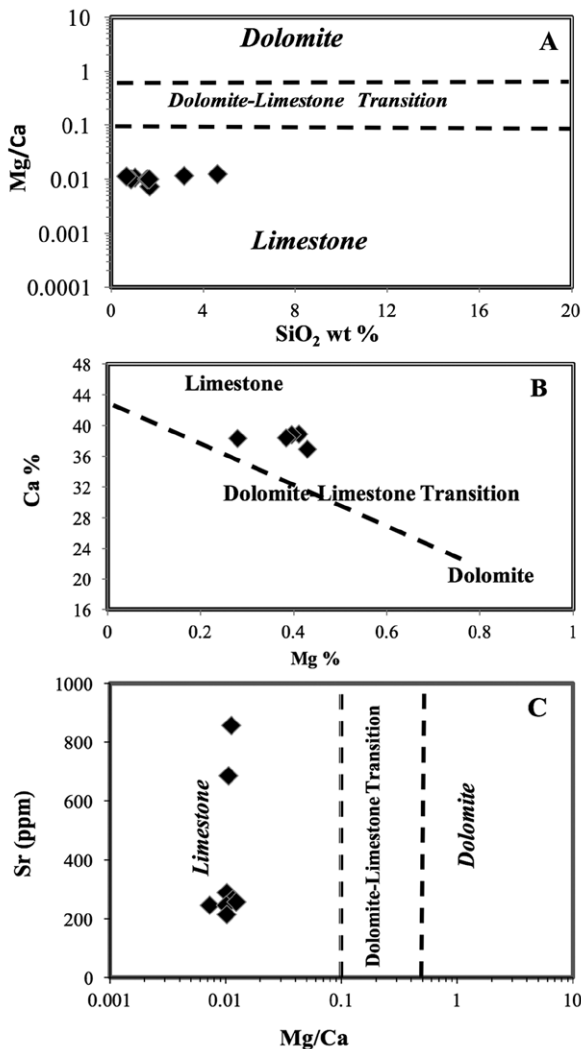


**Figure 7.** Lithological classification based on geochemical data for Gimo marble samples (after Melezhik et al., 2008); **A.** Mg/Ca vs.  $SiO_2$  diagram, **B.** Mg vs. Ca diagram, and **C.** Mg/Ca vs. Sr diagram.

In addition, the studied samples show a moderate concentration of Sr of 382.6 ppm (Table 2), and by using the Sr vs. Mg/Ca plot, the samples are projected in the field of limestone (Fig. 7C). The  $SiO_2$  content of some Gimo marbles exceeded 1 wt.% (Fig. 7A and Table 1), which is attributed to the presence of quartz veinlets and some silicate mineral such as chlorite that were identified by petrographic examination (Fig. 3).

The alkali content of carbonate rocks decreases with an increase in salinity and depth (Clarke, 1911). In general, the composition of a metacarbonate is largely controlled by the distance of its formation from the nearest continent and the topographic elevation at which it is deposited, as well as whether volcanism occurred nearby. All geochemical features of Gimo marbles are characteristic of limestone deposition in a continental basin (Zhang et al., 2017). The very low alkali content ( $Na_2O + K_2O < 0.1$  wt.%) in the studied marbles indicates that the limestone protolith formed in a shallow, saline environment and was later metamorphosed.

In general, a high silica content of a limestone indicates that the basin of deposition of the protolith is near the shoreline (Brownlow, 1996); however, it sometimes reflects the inclusion of quartz veins and veinlets that form after deposition of the precursor sediment. In general, the silica content of marble is related to the availability of silicate minerals and chert nodules, which are produced as impurities in the protolith that may be formed after the deposition of the protolith or during metamorphism (Obasi and Madukwe, 2016; Mirza, 2019; Mirza, 2021). The petrographic study of the Gimo marble revealed the presence of quartz veinlets (Fig. 3F); hence, the silica content is mostly attributed to epigenetic events.

Useful information about the depositional environment of limestone can be provided by LILE ratios (Zhang et al., 2017). A ternary diagram of Rb–Sr–Ba can be used to distinguish limestones deposited in the open ocean, inland freshwater bodies, and continental margins (Fig. 8A). In general, marine limestones that form on continental margins can be distinguished from inland freshwater limestones based on their different Sr/Ba and Sr/Rb ratios, whereby both values are higher in continental margin limestones than in inland freshwater limestones (Fig. 8B). In the case of Gimo marble, all the studied samples are projected in the continental margin field.

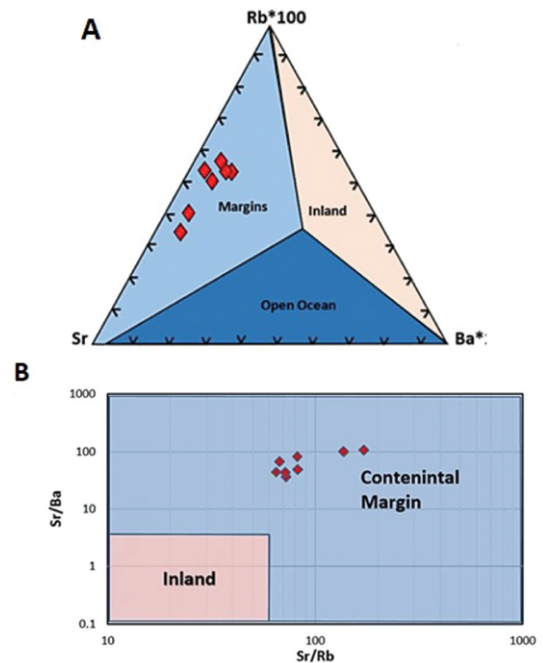


**Figure 8.** **A.** Rb–Sr–Ba ternary diagram and **B.** Sr/Ba vs. Sr/Rb discrimination diagram for limestones indicating a continental margin depositional environment for Gimo marble samples (after Zhang et al., 2017).

The enrichment and depletion of REE in carbonate rock may be influenced by various factors: (i) addition of terrigenous particles from the continent (McLennan, 1989), (ii) scavenging processes related to depth, salinity, and oxygen levels (Elderfield, 1988); (iii) biogenic sedimentation from the

overlying seawater (Murphy and Dymond, 1984), and (v) authigenic removal of REE from the water column and early diagenesis (Sholkovitz, 1988).

REEs are relatively immobile during post-depositional processes, such as diagenesis (Cullers et al., 1979) and metamorphism (Muecke, 1979). To confirm the sedimentary nature of the protolith, it is necessary to investigate the geological characteristics of its depositional environment, which can be achieved in this case by assessing the trace element and REE concentrations. Haskin et al. (1966) and Jarvis et al. (1975) showed that the enrichment of REEs in marbles is positively correlated with the proportion of insoluble substances, such as quartz, clay, mica, silicate, and iron minerals.

According to Tanaka and Kawabe (2006), unaltered marine sedimentary carbonates are expected to preserve the chemical characteristics (i.e. REE ratios) of the medium in which the carbonates precipitated. However, care must be taken when interpreting REE contents in marbles, as they may also be influenced by the presence of non-carbonate materials, such as fine-grained siliciclastic material, especially when present in excess of 5 vol.% (Banner et al., 1988). Fortunately, petrographic and geochemical observations of the Gimo marble show that only negligible amounts of non-carbonate phases occur, and hence their impact on REE patterns can be assumed to be insignificant. In addition, the very low Er/Nd ratio (0.13–0.16) suggests that the Gimo marble is only very slightly influenced by the geochemistry of detrital materials. Tanaka et al. (1990) observed that concentrations of La, Nd, Sm, and Eu in coastal waters have a decreasing linear relationship, and the REE patterns of these waters are characterized by a marked discontinuity between Eu and Gd. Similar features are present for the REE patterns of the Gimo marble (Fig. 6), which indicates that their protoliths were deposited in a shallow, near-shore marine environment. This interpretation agrees with the negligible amounts of Na<sub>2</sub>O, Fe<sub>2</sub>O<sub>3</sub>, and MnO measured in the samples (Table 1) (Clarke, 1911; Turekiah and Wedepohl, 1961; Frank, 1975).

According to Zhang et al. (2017), the  $\Sigma$ REE of oceanic plateau carbonates is 1.31 ppm, but it is 10–30 ppm for carbonates deposited along continental margins and in continental interiors. The REE content of the studied samples ranged from 10.61 to 34.95 ppm; hence, it is interpreted that the studied samples formed in a continental margin setting.

Boulvais et al. (2000) suggested that the REE distribution in marbles varies depending on the degree of fluid interaction that limestone experiences, such that patterns in these elements can be used to understand the nature of fluid flow during metamorphism.

According to Shields and Webb (2004) and Shields and Stille (2001), progressive REE scavenging during post-depositional modification may produce a positive correlation between the Ce anomaly and REE. However, the studied samples display a notable negative correlation between Ce/Ce\* and total REE content (Fig. 9A), implying that such a diagenetic influence is absent. In addition, the correlation between Eu/Eu\* and  $\Sigma$ REE in Fig. 9B highlights the enrichment of Eu in carbonate minerals and depletion of Eu in other minerals, which is interpreted to record Eu removal during metamorphism by the reduction of Eu<sup>3+</sup> to Eu<sup>2+</sup> (Jarvis, et al., 1975). The positive La/La\* anomalies (average 3.64) and slightly flat Pr/Pr\* anomalies (average 1.42), which are plotted in area IIIb of the Pr/Pr\* vs. Ce/Ce\* scatter plot (Fig. 9C) confirm that the Ce anomalies are not a relic of La interference.

The significant negative Ce anomalies and slight positive Gd anomalies observed in the Gimo marbles (Table 3 and Fig. 6) indicate that their protoliths were carbonate rocks of sedimentary origin, and that they were deposited in marine environments (Özyurt et al., 2020). In addition, it has been suggested that a pronounced negative Ce\* anomaly can be divided into three zones: (a) <0.5, (b) ~0.6–0.9, and (c) ~0.9–1.0 which represent oxic, suboxic and anoxic marine water, respectively (Chen et al., 2015). The Ce/Ce\* anomaly of the studied samples ranges between 0.38 and 0.62 (with an average value of 0.48), indicating the oxidation of Ce<sup>3+</sup> to less soluble Ce<sup>4+</sup> that was removed continuously by scavenging (Sholkovitz et al., 1994; Tobia and Mustafa, 2019). Accordingly, the protolith of the studied samples was deposited in an oxygenated environment. A comparison of the REE contents of shallow marine carbonate rocks presented by Özyurt et al. (2020) with those found in this study, show that the studied Gimo samples exhibit the same pattern with strong fractionation of LREE over HREE with a negative Ce anomaly (Fig. 6).

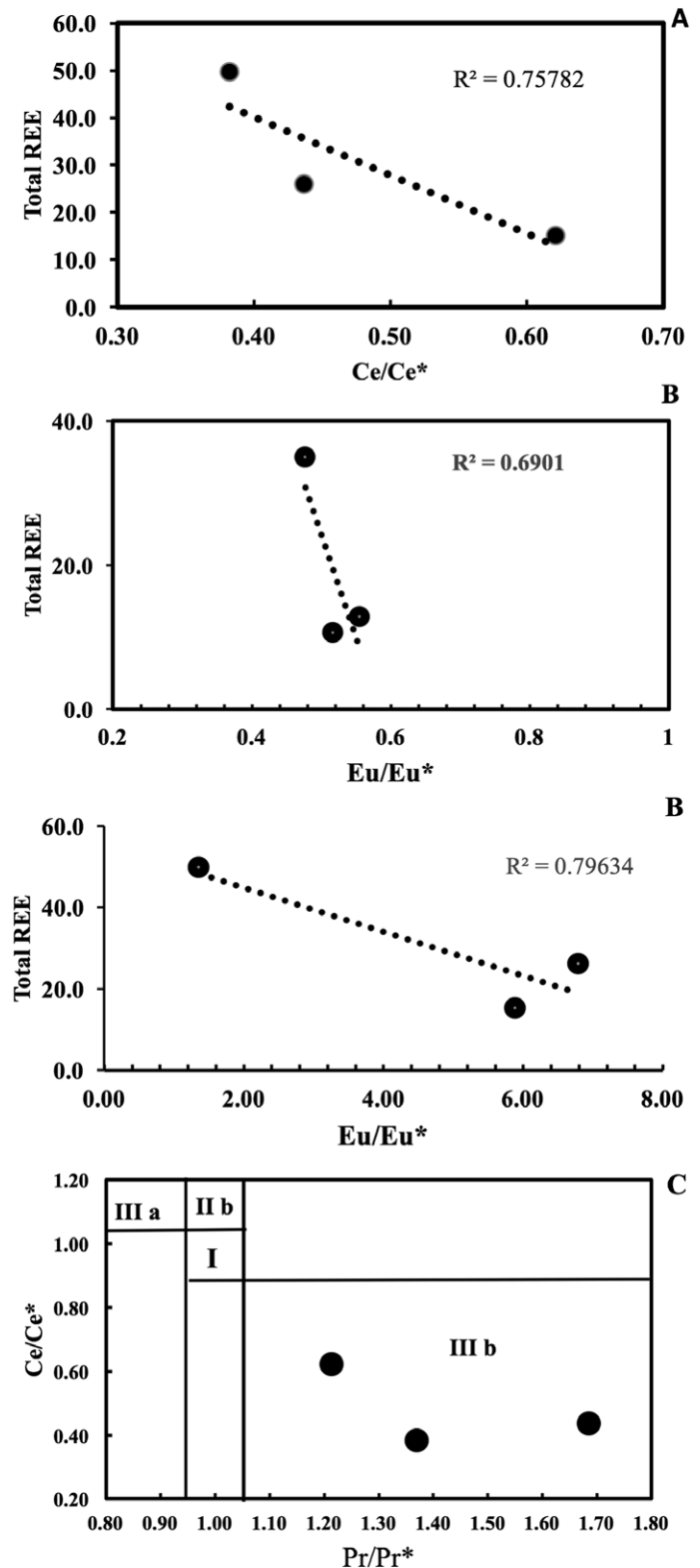


**Figure 9.** Variation diagram of  $\Sigma$ REE content vs. A. Ce/Ce\* and B. Eu/Eu\* for Gimo marble samples. Ce/Ce\* =  $c_{e_N} / (2Pr_N - Nd_N)$ ; Eu/Eu\* =  $Eu_N / (Sm_N + Gd_N)^{0.5}$ , where subscript N refers to normalised values taken from Taylor and McLennan (1985). C. Ce/Ce\* vs. Pr/Pr\* ratios diagram from Bau and Dulski (1996)

It is also notable that the La–Nd–Sm–Eu contents of the Gimo samples define an inclined straight line and HREE (Gd–Dy–Tm–Er–Yb–Lu) contents show more flat patterns (Fig. 6). A low Er/Nd ratio (0.13–0.16) indicates that minor detrital material was present in the protolith.

The Y/Ho ratio can be used as a tracer to assess whether carbonate samples reflect primary marine signatures or siliciclastic components (Nozaki et al., 1997). According to Nozaki et al. (1997) and Zhang and Nozaki (1998), and high Y/Ho ratios (average of  $61 \pm 12$ ) occur in the upper 200 m of seawater. However, other studies have proposed that typical Y/Ho ratios in marine carbonates that are free of contamination from terrigenous material show a wider range of values (44–74) or a chondritic value of 28 (Bau 1996, and Liu et al., 2019). The studied samples display high Y/Ho ratios with an average of 72.30 (40.0–132.0), which is consistent with detritus-free marine sediments (average 45.5), and defined as super chondritic.

Davou and Ashano (2009) reported that low concentrations of  $\text{Na}_2\text{O}$  in marble indicate a shallow, near-shore, low energy, and 'clean water' marine environment of deposition for the protolith. A low  $\text{Al}_2\text{O}_3$  concentration is also interpreted as indicating a low-energy environment.

Finally, several trace elements, including Zr, Hf, Th, and  $\text{Al}_2\text{O}_3$ , are considered to be particularly sensitive to shale contamination, as they occur in detrital alumina silicate minerals in much greater volume in average shale than in marine carbonate (Özyurt et al., 2020). The studied samples predominantly exhibited low Th (< 3 ppm), Hf (< 4 ppm), and Zr (< 22 ppm) contents, which supports the observation that contamination by detrital minerals is minor to negligible (Table 2). The constraints on the pre-metamorphic parent material of the Gimo marbles were derived from the discrimination plot of  $\text{Na}_2\text{O}/\text{Al}_2\text{O}_3$  vs.  $\text{K}_2\text{O}/\text{Al}_2\text{O}_3$  of Garrels and Mckenzie (1971), which shows that the studied marble samples fall within the field of sedimentary and metasedimentary rocks (Fig. 10A). The  $\text{MgO}$ – $\text{CaO}$ – $\text{Al}_2\text{O}_3$  discrimination diagram of Leyreloup et al. (1977) (Fig. 10B) also supports a sedimentary origin, as the studied samples plot outside of the field defining a magmatic origin.

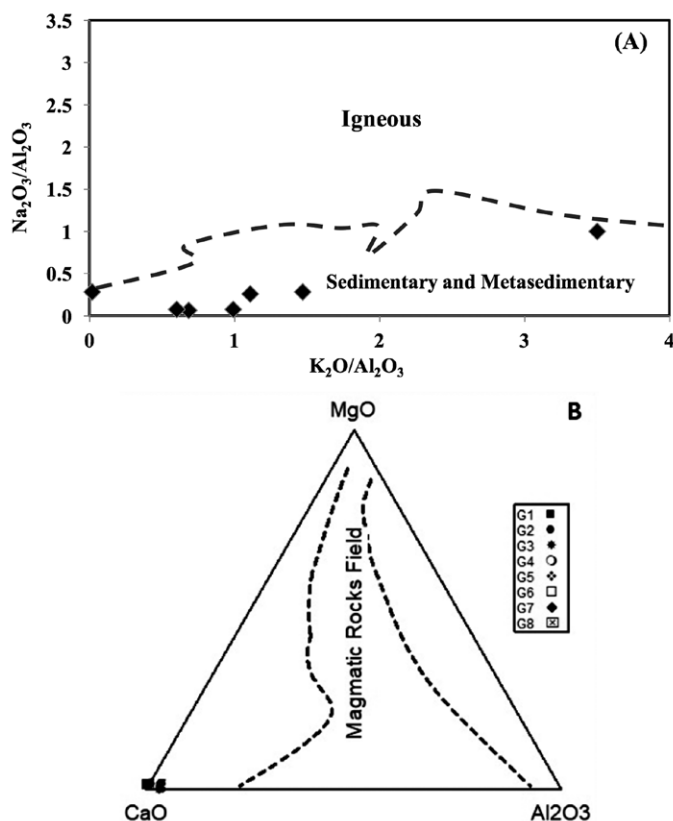


**Figure 10.** A.  $\text{Na}_2\text{O}/\text{Al}_2\text{O}_3$  vs.  $\text{K}_2\text{O}/\text{Al}_2\text{O}_3$  diagram for Gimo marble samples (after Garrels and Mackenzie, 1971); and B. Compositions of Gimo marble samples on a  $\text{MgO}$ – $\text{CaO}$ – $\text{Al}_2\text{O}_3$  discrimination diagram (after Leyreloup et al., 1977).

## 6. Conclusions

1. From a petrographic perspective, the white and grey-colored Gimo marbles display similar mineralogical assemblages and mostly have homeoblastic and mosaic textures. Carbonate minerals (calcite), quartz, chlorite, and ferric iron oxides and sulphides occur in trace amounts as accessory minerals.
2. The mineralogical and geochemical data correlate well with each other, suggesting that all marbles formed from the same source and/or the same geological process controlled the bulk composition. In addition, both field observations and the application of geochemical indices indicate that the Gimo marble is of sedimentary and metasedimentary origin.
3. The absence of dolomite in the Gimo marble indicates that the protolith of the studied samples was a relatively pure limestone prior to its metamorphism.
4. The very low content of Th, Hf, and Zr in Gimo marble supports that contamination by detrital minerals is minor to negligible.
5. The PAAS-normalised REE distribution patterns reveal slight enrichment in HREE, with negative Ce, and positive La anomalies (average  $\text{La}/\text{La}^* = 3.64$ ) and a super chondritic Y/Ho ratio (average 72.3).
6. The Ce/C\* vs. Pr/Pr\* relationships and the position of the studied samples in area IIIb indicate that they display real Ce anomalies and not an artefact of La interference.
7. The REE pattern of the studied samples indicates that the protolith limestone formed in a continental margin setting. In addition, the significant negative Ce anomaly indicates that the protolith of Gimo marbles was a carbonate rock with a sedimentary origin that was deposited in an oxygenated marine environment.

## Acknowledgement

The authors would like to thank Dr. V. Xanthopoulou, Laboratory of Electron Microscopy and Microanalysis, Faculty of Natural Sciences, University of Patras, for conducting the XRF analysis.

## References

- Alavi, M. (1994). Tectonics of the Zagros orogenic belt of Iran: new data and interpretations. *Tectonophysics*, 229(3-4), 211-238. [https://doi.org/10.1016/0040-1951\(94\)90030-2](https://doi.org/10.1016/0040-1951(94)90030-2)
- Ali, S. A., Ismail, S. A., Nutman, A. P., Bennett, V. C., Jones, B. G., & Buckman, S. (2016). The intra-oceanic Cretaceous (~ 108 Ma) Kata-Rash arc fragment in the Kurdistan segment of Iraqi Zagros suture zone: Implications for Neotethys evolution and closure. *Lithos*, 260, 154-163. DOI:10.1016/j.lithos.2016.05.027
- Amrouni, K. S., Shaltami, O. R., El-Hawat, A. S., Pope, M. C., Amer, A., Elbileikia, E. A., ... & Wehner, M. P. (2018). Geochemical Analysis of the Carbonate-Evaporite Miocene Outcrops in the Cyrenaica Region of Libya: Cyrenaica Platform and Sirt Basin. *Gulf Coast Association of Geological Societies*, 68, 35-49.
- Aswad, K. J. (1999). Arc-continent collision in Northeastern Iraq as evidenced by Mawat and Penjwin Ophiolite Complexes. *Raffidain Journal of Science*, 10, 51-61.
- Aswad, K. J., Aziz, N. R., & Koyi, H. A. (2011). Cr-spinel compositions in serpentinites and their implications for the petro-tectonic history of the Zagros Suture Zone, Kurdistan Region, Iraq. *Geological magazine*, 148(5-6), 802-818. <https://doi.org/10.1017/S0016756811000422>
- Aswad, K. J., & Elias, E. M. (1988). Petrogenesis, geochemistry and metamorphism of spilitized subvolcanic rocks of the Mawat Ophiolite Complex, NE Iraq. *Ofoliti*, 13(2/3), 95-109.
- Awadh, S. M. (1991). Petrology and geochemistry of the Shalair Metamorphic Rock Group. Shalair Valley area. Northeastern Iraq. Master thesis (Unpublished). Baghdad University, Science college, Iraq.

- Awadh, S. M., & Kettanah, Y. (2008). Petrology, Geochemistry and Tectonical Environment of The Shalair Metamorphic Rock Group and Katar Rash Volcanic Group, Shalair Vally area, Northeastern Iraq. *Iraqi Journal of Science*, 49(1), 149-158.
- Banner, J. L., Hanson, G. N., & Meyers, W. J. (1988). Rare earth element and Nd isotopic variations in regionally extensive dolomites from the Burlington-Keokuk Formation (Mississippian); implications for REE mobility during carbonate diagenesis. *Journal of Sedimentary Research*, 58(3), 415-432. <https://doi.org/10.1306/212F8DAA-2B24-11D7-8648000102C1865D>
- Barker, A. J. (2014). *A key for identification of rock-forming minerals in thin section*. CRC Press. London, UK. 182pp.
- Bau, M., & Dulski, P. (1996). Distribution of yttrium and rare-earth elements in the Penge and Kuruman iron-formations, Transvaal Supergroup, South Africa. *Precambrian Research*, 79(1-2), 37-55. [https://doi.org/10.1016/0301-9268\(95\)00087-9](https://doi.org/10.1016/0301-9268(95)00087-9)
- Bau, M. (1996). Controls on the fractionation of isoivalent trace elements in magmatic and aqueous systems: evidence from Y/Ho, Zr/Hf, and lanthanide tetrad effect. *Contributions to Mineralogy and Petrology*, 123(3), 323-333. <https://doi.org/10.1007/s004100050159>
- Bolton, C. M. G. (1958). *The geology of the Ranya. Site investigation co – report*. NIMCO Lib. Unpublished report, Baghdad, Iraq.
- Boulvais, P., Fourcade, S., Moine, B., Gruau, G., & Cuney, M. (2000). Rare-earth elements distribution in granulite-facies marbles: a witness of fluid-rock interaction. *Lithos*, 53(2), 117-126. DOI:10.1016/S0024-4937(00)00013-X
- Brownlow, A. H. (1996). *1996: Geochemistry*. Upper Saddle River, NJ: Prentice-Hall. pp. 350-351.
- Buday, T. (1980). *The regional geology of Iraq: tectonism, magmatism and metamorphism* (Vol. 2). State Organization for Minerals, Directorate General for Geological Survey and Mineral Investigations.
- Buday, E., & Blackman, S. (1975). Hot food merchandiser U.S. Patent No. 3,911,248. Washington, DC: U.S. Patent and Trademark Office.
- Buday, T., & Jassim, S. Z. (1987). The Regional Geology of Iraq. Vol. 2, Tectonism, Magmatism and Metasomatism. Kassab, IM, and Abbas. *DG Geol. Surv. Min. Invest., lib. Published, Baghdad, Iraq*. 352p.
- Chen, J., Algeo, T. J., Zhao, L., Chen, Z. Q., Cao, L., Zhang, L., & Li, Y. (2015). Diagenetic uptake of rare earth elements by bioapatite, with an example from Lower Triassic conodonts of South China. *Earth-science reviews*, 149, 181-202. <https://doi.org/10.1016/j.earscirev.2015.01.013>
- Clarke, F. N. (1911). *The data of geochemistry*. 2nd ed., Washington Government Printing Press: 782p.
- Cullers, R., Chaudhuri, S., Kilbane, N., & Koch, R. (1979). Rare-earths in size fractions and sedimentary rocks of Pennsylvanian-Permian age from the mid-continent of the USA. *Geochimica et Cosmochimica Acta*, 43(8), 1285-1301. [https://doi.org/10.1016/0016-7037\(79\)90119-4](https://doi.org/10.1016/0016-7037(79)90119-4)
- Davou, D. D., & Ashano, E. C. (2009). The geochemical chararateristics of the marble deposits east of Federal Capital Territory (FCT), Nigeria. *Global Journal of Geological Sciences*, 7(2). DOI:10.4314/gjgs.v7i2.51608
- DeVilliers, P. R. (1975). *Geology of the Shalair Valley*. SOM Lib., Baghdad, 270152
- De Vera, J., Gines, J., Oehlers, M., McClay, K., & Doski, J. (2009). Structure of the Zagros fold and thrust belt in the Kurdistan Region, northern Iraq. *Trabajos de geología*, (29).
- Dypvik, H., & Harris, N. B. (2001). Geochemical facies analysis of fine-grained siliciclastics using Th/U, Zr/Rb and (Zr+ Rb)/Sr ratios. *Chemical geology*, 181(1-4), 131-146. DOI: 10.1016/S0009-2541(01)00278-9
- Elderfield, H. (1988). The oceanic chemistry of the rare-earth elements. *Philosophical Transactions of the Royal Society of London. Series A, Mathematical and Physical Sciences*, 325(1583), 105-126. <https://doi.org/10.1098/rsta.1988.0046>
- Ephraim, B. E. (2012). Investigation of the geochemical signatures and conditions of formation of metacarbonate rocks occurring within the Mamfe embayment of south-eastern Nigeria. *Earth Sciences Research Journal*, 16(2), 121-138.
- Ferrill, D. A., Morris, A. P., Evans, M. A., Burkhard, M., Groshong Jr, R. H., & Onasch, C. M. (2004). Calcite twin morphology: a low-temperature deformation geothermometer. *Journal of structural Geology*, 26(8), 1521-1529. <https://doi.org/10.1016/j.jsg.2003.11.028>
- Frank, W. (1975). Sediment Chemische and Palolcologische Asperkte Stablier Schewellen. *Ben Sonderforschungsberoch*, 48, 31-40.
- Frimmel, H. E. (2009). Trace element distribution in Neoproterozoic carbonates as palaeoenvironmental indicator. *Chemical Geology*, 258(3-4), 338-353. <https://doi.org/10.1016/j.chemgeo.2008.10.033>
- Garrels, R. M., & Mckenzie, F. T. (1971). *Evolution of sedimentary rocks*. WW Worton and Co. Inc. New York, 394.
- Georgieva, M., Cherneva, Z., Hekimova, S., & Petrova, A. (2009). Petrology of marbles from the Arda tectonic unit, Central Rhodope, Bulgaria. *National conference, Geosciences*.
- Goldschmidt, J. R., Graff, L., & Joensu, O. I. (1955). The occurrence of magnesium calcite in nature. *Geochimica et Cosmochimica Acta*, 1, 212-230. [https://doi.org/10.1016/0016-7037\(55\)90033-8](https://doi.org/10.1016/0016-7037(55)90033-8)
- Haskin, L. A., Wildeman, T. R., Frey, F. A., Collins, K. A., Keedy, C. R., & Haskin, M. A. (1966). Rare earths in sediments. *Journal of Geophysical Research*, 71(24), 6091-6105. <https://doi.org/10.1029/JZ071i024p06091>
- Jassim, S. Z., & Goff, J. C. (2006). *Geology of Iraq*. DOLIN, sro, distributed by Geological Society of London. 341pp.
- Jassim, S. Z., & MI, A. H. (1977). Petrography and origin of the Mawat and Penjwin Igneous Complex: a comparison. *Journal of the Geological Society of Iraq*, special issue, 169-210.
- Jassim, Z., Buda, G., Neuzilova, M., & Suk, M. (1982). Metamorphic development of the Iraqi Zagros ophiolite zone. *Krystalinikum*, 16, 21-40.
- Jarvis, J. C., Wildeman, T. R., & Banks, N. G. (1975). Rare earths in the Leadville limestone and its marble derivatives. *Chemical Geology*, 16(1), 27-37. [https://doi.org/10.1016/0009-2541\(75\)90088-1](https://doi.org/10.1016/0009-2541(75)90088-1)
- Kandemir, R., & Yilmaz, C. (2009). Lithostratigraphy, facies, and deposition environment of the lower Jurassic Ammonitico Rosso type sediments (ARTS) in the Gümüşhane area, NE Turkey: implications for the opening of the northern branch of the Neo-Tethys Ocean. *Journal of Asian Earth Sciences*, 34(4), 586-598. DOI:10.1016/j.jseaes.2008.08.006
- Karim, K. H. (2004). Origin of structures and textures of some Kurdistan marbles as inferred from sedimentary ancestor structures, NE-Iraq. *Journal of Zankoy Sulaimani*, 7(1) Part A, 69-86.
- Konrad, B. K. & Dennis, K. B. (1995). *Introduction to geochemistry*. 3rd ed. McGraw-Hill Book Co., Singapore, 250p
- Leyreloup, A. (1977). Chemical composition and consequences of the evolution of the French massif central Precambrian crust. *Contributions to Mineralogy and Petrology*, 62, 283-300.
- Liu, J., Song, J., Yuan, H., Li, X., Li, N., & Duan, L. (2019). Rare earth element and yttrium geochemistry in sinking particles and sediments of the Jiaozhou Bay, North China: Potential proxy assessment for sediment resuspension. *Marine Pollution Bulletin*, 144, 79-91. <https://doi.org/10.1016/j.marpolbul.2019.04.044>
- McLennan, S. M. (1989). Rare earth elements in sedimentary rocks: influence of provenance and sedimentary processes. *Geochemistry and mineralogy of rare earth elements, reviews in mineralogy* 21, 169-200.
- McLennan, S. M. (2001). Relationships between the trace element composition of sedimentary rocks and upper continental crust. *Geochemistry, Geophysics, Geosystems*, 2(4). <https://doi.org/10.1029/2000GC000109>
- Melezhik, V. A., Bingen, B., Fallick, A. E., Gorokhov, I. M., Kuznetsov, A. B., Sandstad, J. S., ... & Moniz, A. (2008). Isotope chemostratigraphy of marbles in northeastern Mozambique: apparent depositional ages and

- teconostratigraphic implications. *Precambrian Research*, 162(3-4), 540-558. DOI:10.1016/j.precamres.2007.11.002
- Mirza, T. A., Kalaitzidis, S. P., Mohammed, S. H., Rashid, S. G., & Petrou, X. (2017). Geochemistry and genesis of sulphide ore deposits in Sharosh Village, Qandil Series, Kurdistan Region, NE Iraq. *Arabian Journal of Geosciences*, 10(19), 1-19. DOI:10.1007/s12517-017-3210-y
- Mirza, T. A., & Rashid, S. G. (2018). Mineralogy, Fluid inclusions and stable isotopes study constraints on genesis of sulfide ore mineral, Qaladiza area Qandil Series, Iraqi Kurdistan Region. *Arabian Journal of Geosciences*, 11(7), 1-15. DOI:10.1007/s12517-018-3490-x
- Mirza, T. A. (2019). Geochemical and isotopic characteristics of Zangalline marble, Ranya area, Qandil Series, northeastern Iraqi Kurdistan Region: implications for genesis. *Arabian Journal of Geosciences*, 12(4), 1-11. <https://doi.org/10.1007/s12517-019-4284-5>
- Muecke, T. W. (1979). Formation fines and factors controlling their movement in porous media. *Journal of petroleum technology*, 31(02), 144-150. <https://doi.org/10.2118/7007-PA>
- Murphy, K., & Dymond, J. (1984). Rare earth element fluxes and geochemical budget in the eastern equatorial Pacific. *Nature*, 307(5950), 444-447. <https://doi.org/10.1038/307444a0>
- Nozaki, Y., Zhang, J., & Amakawa, H. (1997). The fractionation between Y and Ho in the marine environment. *Earth and Planetary Science Letters*, 148(1-2), 329-340. [https://doi.org/10.1016/S0012-821X\(97\)00034-4](https://doi.org/10.1016/S0012-821X(97)00034-4)
- Obasi, R. A., & Ogungbuyi, P. I. (2013). Petrogenetic and Distribution of Trace and Rare-Earth Elements in the Marble from Igarra Area, Southwest Nigeria. *Journal of Environment and Earth Science*, 3(13), 66-76.
- Obasi, R. A., & Madukwe, H. Y. (2016). Use of geochemistry to study the provenance, tectonic setting, source-area weathering and maturity of Igarra Marble, Southwest, Nigeria. *American Journal of Engineering Research*, 5(6), 90, 99.
- Özyurt, M., Kırmacı, M. Z., Al-Aasm, I., Hollis, C., Taslı, K., & Kandemir, R. (2020). REE Characteristics of Lower Cretaceous Limestone Succession in Gümüşhane, NE Turkey: Implications for Ocean Paleoredox Conditions and Diagenetic Alteration. *Minerals*, 10(8), 683. <https://doi.org/10.3390/min10080683>
- Qadhi, T. M. (2008). Testing Jabal Farasan marble deposit for multiple industrial applications. *Arabian Journal for Science and Engineering*, 33(1C), 79-97.
- Shearman, D. J., & Shirmohammadi, N. H. (1969). Distribution of strontium in dedolomites from the French Jura. *Nature*, 223(5206), 606-608. <https://doi.org/10.1038/223606a0>
- Shields, G., & Stille, P. (2001). Diagenetic constraints on the use of cerium anomalies as palaeoseawater redox proxies: an isotopic and REE study of Cambrian phosphorites. *Chemical Geology*, 175(1-2), 29-48. DOI:10.1016/S0009-2541(00)00362-4
- Shields, G., & Webb, G. (2004). Has the REE composition of seawater changed over geological time?. *Chemical Geology*, 204(1-2), 103-107. <https://doi.org/10.1016/j.chemgeo.2003.09.010>
- Sholkovitz, E. R. (1988). Rare earth elements in the sediments of the North Atlantic Ocean, Amazon Delta, and East China Sea; reinterpretation of terrigenous input patterns to the oceans. *American Journal of Science*, 288(3), 236-281. DOI:10.2475/AJS.288.3.236
- Sholkovitz, E. R., Landing, W. M., & Lewis, B. L. (1994). Ocean particle chemistry: the fractionation of rare earth elements between suspended particles and seawater. *Geochimica et Cosmochimica Acta*, 58(6), 1567-1579. [https://doi.org/10.1016/0016-7037\(94\)90559-2](https://doi.org/10.1016/0016-7037(94)90559-2)
- Smirnov, V. A., & Nelidov, V. P. (1962). *Report on 1: 20000 prospecting correlation of the Sylaimaniya-Choarta and Penjwin area carried out in 1961*. Unpublished report, SOM Lib, Baghdad, 46p.
- Stampfli, G. M., & Borel, G. D. (2002). A plate tectonic model for the Paleozoic and Mesozoic constrained by dynamic plate boundaries and restored synthetic oceanic isochrons. *Earth and Planetary Science Letters*, 196(1-2), 17-33. [https://doi.org/10.1016/S0012-821X\(01\)00588-X](https://doi.org/10.1016/S0012-821X(01)00588-X)
- Storey, C. C., & Vos, M. A. (1981). Industrial minerals of the Pembroke-Renfrew area.
- Taelman, D., Elburg, M., Smet, I., De Paep, P., Lopes, L., Vanhaecke, F., & Vermeulen, F. (2013). Roman marble from Lusitania: petrographic and geochemical characterisation. *Journal of Archaeological Science*, 40(5), 2227-2236. <https://doi.org/10.1016/j.jas.2012.12.030>
- Talbot, C. J., & Alavi, M. (1996). *The past of a future syntaxis across the Zagros*. Geological Society, London, Special Publications, 100(1), 89-109.
- Tanaka, K., & Kawabe, I. (2006). REE abundances in ancient seawater inferred from marine limestone and experimental REE partition coefficients between calcite and aqueous solution. *Geochemical Journal*, 40(5), 425-435. <https://doi.org/10.2343/geochemj.40.425>
- Tanaka, M., Shimizu, H., & Masuda, A. (1990). Features of the heavy rare-earth elements in seawater. *Geochemical Journal*, 24(1), 39-46. <https://doi.org/10.2343/geochemj.24.39>
- Taylor, S. R., & McLennan, S. M. (1985). *The continental crust: its composition and evolution*. Blackwell, Oxford, 312pp.
- Turekian, K. K., & Wedepohl, K. H. (1961). Distribution of the elements in some major units of the earth's crust. *Geological Society of America bulletin*, 72(2), 175-192. [https://doi.org/10.1130/0016-7606\(1961\)72\[175:DOTEIS\]2.0.CO;2](https://doi.org/10.1130/0016-7606(1961)72[175:DOTEIS]2.0.CO;2)
- Tobia, F. H., & Mustafa, B. H. (2019). Provenance and depositional environment of the carbonates from Baluti Formation (Late Triassic), Kurdistan Region, Iraq. *The Iraqi Geological Journal*, 18-35.
- Zhang, K. J., Li, Q. H., Yan, L. L., Zeng, L., Lu, L., Zhang, Y. X., ... & Tang, X. C. (2017). Geochemistry of limestones deposited in various plate tectonic settings. *Earth-Science Reviews*, 167, 27-46. <https://doi.org/10.1016/j.earscirev.2017.02.003>
- Zhang, J., & Nozaki, Y. (1998). Behavior of rare earth elements in seawater at the ocean margin: a study along the slopes of the Sagami and Nankai troughs near Japan. *Geochimica et Cosmochimica Acta*, 62(8), 1307-1317. [https://doi.org/10.1016/S0016-7037\(98\)00073-8](https://doi.org/10.1016/S0016-7037(98)00073-8)